A novel numerical method for the analysis of electron transport in the presence of pointlike magnetic scatterers

2008 J. Phys.: Condens. Matter 20 365208

(http://iopscience.iop.org/0953-8984/20/36/365208)

IOP PUBLISHING JOURNAL OF PHYSICS: CONDENSED MATTER

J. Phys.: Condens. Matter **20** (2008) 365208 (6pp) doi:10.1088/0953-8984/20/36/365208

A novel numerical method for the analysis of electron transport in the presence of pointlike magnetic scatterers

Yuu Miyagawa[1] **and Tsuyoshi Ueta**[2]

[1] Graduate School of Science and Technology, Chiba University, 1-33 Yayoi-cho, Inage-ku, Chiba 263-8522, Japan
[2] Institute of Media and Information Technology, Chiba University, 1-33 Yayoi-cho, Inage-ku, Chiba 263-8522, Japan

E-mail: ueta@faculty.chiba-u.jp

Received 19 April 2008
Published 14 August 2008
Online at stacks.iop.org/JPhysCM/20/365208

Abstract

The boundary element method (BEM) is so extended as to treat two-dimensional (2D) electron systems in the presence of pointlike islands of magnetic moment. In the present paper, the pointlike magnetic scatterer is modeled by a cylindrical barrier. The radius of the cylindrical barrier is assumed to be so small, keeping the volume definite, that the pointlike magnetic scatterer is approximated by a Dirac δ function. Then, we make an approximation on the BEM formulation, wherefore we derive a novel numerical method for electron transport in the presence of pointlike magnetic scatterers. In a numerical implementation of the method extended here, the numerical errors of probability conservation are less than 1% for any cases and the computational costs, that is, the required memory amount and CPU time, are much reduced. As examples, the proposed method is applied to transport problems through a quantum wire with four pointlike magnetic scatterers. It is clearly shown that magnetic scatterers, even pointlike magnetic moments, lead to spin flip-flop, localization and resonance.

1. Introduction

For two decades, the electron transport through a nanostructure such as a quantum dot has attracted much interest. In recent years, a variety of spin-dependent transport phenomena in magnetic nanostructures like magnetic multilayers and magnetic tunnel junctions has been extensively investigated [1, 2]. Magnetic superlattices are fabricated by piling up magnetic and non-magnetic metallic thin films alternately with thicknesses of the order of one nanometer. In such magnetic systems of nanometer size, the interplay between spin and charge of electrons provides unique transport phenomena, such as giant magnetoresistance of the magnetic tunnel effect. The electronics using both the charge and the spin of an electron is called spintronics and shows rapid development [3–5]. For such electron systems with a magnetic barrier region, only simple cases have been investigated theoretically [6, 7].

On the other hand, magnetoresistance anomalies were experimentally observed in 2D electron systems in which periodic potential modulation is introduced artificially, that is a periodic superstructure or an antidot array 15 years or more before [8–10]. For example, oscillation of magnetoresistance as a function of magnetic field strength, the so-called Weiss oscillation, anomalous low-field Hall plateaus and a quenching of the Hall effect about zero magnetic field are observed. In such a case, we can expected that an electron system with an array of magnetic scatterers shows novel phenomena in electron transport.

Actually, a spatially modulated vector potential has been introduced into a 2D electron gas by Xue and Xiao, Yagi and Iye, and Peeters and Vasilopoulos *et al* [11–14]. Then, they have observed a magnetic analogue of the Weiss oscillation. Their strength of the field modulation is so weak that it can be treated as a perturbation. Therefore, no spin flip is observed in such cases.

In the present paper, we attempt to treat theoretically electron transport in a 2D electron gas with a lot of magnetic scatterers [15]. In particular, we focus on the spin flip-flop of a conducting electron.

Now, we consider pointlike magnetic scatterers. Then, the BEM is extended for the case that a lot of pointlike magnetic

moments exist in a ballistic 2D electron system [16]. In the proposed method, additional unknown variables of only the same number as that of the scatterers are required, whereas both memory and CPU time are saved.

The method extended here is applied to a quantum wire with pointlike magnetic scatterers as an example of the application. Transmission and reflection spectra are computed for some cases and the electron density plots allow us to see directly that magnetic scatterers, even several pointlike magnetic moments, lead to spin flip, localization and resonance.

2. Boundary integral equation

We assume that the conduction electrons are polarized in the direction of the z axis, that is, perpendicular to the 2D electron systems. According to Slonczewski [6], the electron wave propagation in a system with magnetization is described by the Schrödinger equation in dimensionless form as

$$\left(-\nabla^2 - \boldsymbol{\sigma}\cdot\boldsymbol{M}(\boldsymbol{r})\right)\begin{pmatrix}\psi_+\\ \psi_-\end{pmatrix} = k^2\begin{pmatrix}\psi_+\\ \psi_-\end{pmatrix}, \tag{1}$$

where ψ_+ and ψ_- are the wavefunctions for up spin or down spin, respectively, k is the wavenumber and $\boldsymbol{\sigma} = (\sigma_x, \sigma_y, \sigma_z)$ are the Pauli spin matrices. The vector $\boldsymbol{M}(\boldsymbol{r}) = (M_x(\boldsymbol{r}), M_y(\boldsymbol{r}), M_z(\boldsymbol{r}))$ is the magnetization or the molecular field of scatterers.

If we employ the usual expression for the Pauli spin matrices, that is:

$$\sigma_x = \begin{pmatrix}0 & 1\\ 1 & 0\end{pmatrix}, \qquad \sigma_y = \begin{pmatrix}0 & -\mathrm{i}\\ \mathrm{i} & 0\end{pmatrix},$$
$$\sigma_z = \begin{pmatrix}1 & 0\\ 0 & -1\end{pmatrix},$$

equation (1) becomes

$$-\nabla'^2\psi_\pm(\boldsymbol{r}') - \left(M_x(\boldsymbol{r}') \mp \mathrm{i}M_y(\boldsymbol{r}')\right)\psi_\mp(\boldsymbol{r}') = \left(k^2 \pm M_z(\boldsymbol{r}')\right)\psi_\pm(\boldsymbol{r}'). \tag{2}$$

By means of the Green function $G(\boldsymbol{r}, \boldsymbol{r}'; \varepsilon)$ satisfying the equation

$$-\nabla'^2 G(\boldsymbol{r}, \boldsymbol{r}'; \varepsilon) = \varepsilon G(\boldsymbol{r}, \boldsymbol{r}'; \varepsilon) + \delta(\boldsymbol{r} - \boldsymbol{r}'), \tag{3}$$

and the boundary condition for the outgoing wave, the wavefunction $\psi_\pm(\boldsymbol{r})$ within a closed boundary is expressed by the boundary integral:

$$\psi_\pm(\boldsymbol{r}) = \oint\left[G(\boldsymbol{r}, \boldsymbol{r}'; k^2)\nabla'\psi_\pm(\boldsymbol{r}') - \psi_\pm(\boldsymbol{r}')\nabla' G(\boldsymbol{r}, \boldsymbol{r}'; k^2)\right]\cdot\boldsymbol{n}\,\mathrm{d}S' + \int G(\boldsymbol{r}, \boldsymbol{r}')\left(M_\mp(\boldsymbol{r}')\psi_\mp(\boldsymbol{r}') \pm M_z(\boldsymbol{r}')\psi_\pm(\boldsymbol{r}')\right)\mathrm{d}\boldsymbol{r}', \tag{4}$$

where $\boldsymbol{n}$ is the unit outward normal vector on the boundary and $M_\pm(\boldsymbol{r}') \equiv M_x(\boldsymbol{r}') \pm \mathrm{i}M_y(\boldsymbol{r}')$. The Green function $G(\boldsymbol{r}, \boldsymbol{r}'; \varepsilon)$ of equation (3) is given by the zeroth-order Hankel function of the first kind as

$$G(\boldsymbol{r}, \boldsymbol{r}'; k^2) = \frac{\mathrm{i}}{4}H_0^{(1)}\left(k|\boldsymbol{r} - \boldsymbol{r}'|\right). \tag{5}$$

In order to apply the BEM, we need to evaluate the volume integral of the last term on the right-hand side.

3. Approximation

Here, we consider N pointlike scatterers of the same small scattering area. The scatterer is modeled by a cylindrical barrier of finite height $\mathcal{M}_\pm(\boldsymbol{R})$ and $\mathcal{M}_z(\boldsymbol{R})$, where a is the radius of the cylindrical barrier, so that the total magnetization is written as

$$M_\pm(\boldsymbol{r}) = \sum_{n=1}^{N}\mathcal{M}_\pm(\boldsymbol{R}_n)a^2\frac{1}{\pi a^2}\theta(a - |\boldsymbol{r} - \boldsymbol{R}_n|)$$
$$M_z(\boldsymbol{r}) = \sum_{n=1}^{N}\mathcal{M}_z(\boldsymbol{R}_n)a^2\frac{1}{\pi a^2}\theta(a - |\boldsymbol{r} - \boldsymbol{R}_n|), \tag{6}$$

where $\boldsymbol{R}_n$ is the position vector of the center of the nth scatterer, $\mathcal{M}_\pm(\boldsymbol{R}_n) \equiv \mathcal{M}_x(\boldsymbol{R}_n) \pm \mathrm{i}\mathcal{M}_y(\boldsymbol{R}_n)$ is defined and $\theta(x)$ is the unit step function. We make the radius a small enough keeping $\mathfrak{M}a^2 \equiv |\mathcal{M}_\pm|a^2$ and $\mathcal{M}_z a^2$ constant, since now we are considering pointlike scatterers. The scattering potential $(1/\pi a^2)\theta(a - |\boldsymbol{r} - \boldsymbol{R}_n|)$ may then be approximated by Dirac's δ function $\delta(\boldsymbol{r} - \boldsymbol{R}_n)$. Therefore, the term on the right-hand side of equation (4) can be evaluated as

$$\begin{aligned}
&\int G(\boldsymbol{r}, \boldsymbol{r}')\left(M_\mp(\boldsymbol{r}')\psi_\mp(\boldsymbol{r}') \pm M_z(\boldsymbol{r}')\psi_\pm(\boldsymbol{r}')\right)\mathrm{d}\boldsymbol{r}'\\
&= \sum_{n=1}^{N}\mathcal{M}_\mp(\boldsymbol{R}_n)a^2\int G(\boldsymbol{r}, \boldsymbol{r}')\\
&\quad\times\frac{1}{\pi a^2}\theta(a - |\boldsymbol{r}' - \boldsymbol{R}_n|)\psi_\mp(\boldsymbol{r}')\,\mathrm{d}\boldsymbol{r}'\\
&\quad\pm\mathcal{M}_z(\boldsymbol{R}_n)a^2\int G(\boldsymbol{r}, \boldsymbol{r}')\\
&\quad\times\frac{1}{\pi a^2}\theta(a - |\boldsymbol{r}' - \boldsymbol{R}_n|)\psi_\pm(\boldsymbol{r}')\,\mathrm{d}\boldsymbol{r}'\\
&\approx \sum_{n} G(\boldsymbol{r}, \boldsymbol{R}_n)\left(\mathcal{M}_\mp(\boldsymbol{R}_n)a^2\psi_\mp(\boldsymbol{R}_n)\right.\\
&\quad\left.\pm\mathcal{M}_z(\boldsymbol{R}_n)a^2\psi_\pm(\boldsymbol{R}_n)\right).
\end{aligned} \tag{7}$$

In the summation of equation (7), if $\boldsymbol{r}$ is set on $\boldsymbol{R}_m$, $G(\boldsymbol{R}_m, \boldsymbol{R}_m)$ is divergent due to the singularity of the Green function. Therefore, when we take $\boldsymbol{r}$ as $\boldsymbol{R}_m$, we need to evaluate the volume integral in equation (4):

$$\frac{1}{\pi a^2}\int G(\boldsymbol{R}_m, \boldsymbol{r}')\theta(a - |\boldsymbol{r}' - \boldsymbol{R}_m|)\psi_\pm(\boldsymbol{r}')\,\mathrm{d}\boldsymbol{r}' = \frac{1}{\pi a^2}\int\frac{\mathrm{i}}{4}H_0^{(1)}(k|\boldsymbol{R}_m - \boldsymbol{r}'|)\theta(a - |\boldsymbol{r}' - \boldsymbol{R}_m|)\psi_\pm(\boldsymbol{r}')\,\mathrm{d}\boldsymbol{r}'$$

more accurately in order to avoid the divergence.

Now, considering the small scattering radius a, we can reasonably evaluate the Hankel function in the integral as

$$H_0^{(1)}(z) \approx 1 + \mathrm{i}\frac{2}{\pi}\left(\ln z + \gamma - \ln 2\right), \tag{8}$$

where γ is Euler's constant [17]. The wavefunction $\psi_\pm(\boldsymbol{r}')$ in the integrand may be taken outside the integral, since the wavefunction $\psi_\pm(\boldsymbol{r}')$ in the integrand should not vary very far from the value at the center $\boldsymbol{R}_m$ within the range in which the step function has a definite value. We may then write $\psi_\pm(\boldsymbol{r}') \approx \psi_\pm(\boldsymbol{R}_m)$, so that the volume integral is estimated as

$$\begin{aligned}
&\frac{1}{\pi a^2}\int G(\boldsymbol{R}_m,\boldsymbol{r}')\theta(a-|\boldsymbol{r}'-\boldsymbol{R}_m|)\psi_\pm(\boldsymbol{r}')\,\mathrm{d}\boldsymbol{r}' \\
&\quad\approx \frac{\mathrm{i}}{4\pi a^2}\psi_\pm(\boldsymbol{R}_m)\int H_0^{(1)}\left(k|\boldsymbol{r}'-\boldsymbol{R}_m|\right) \\
&\qquad\times\theta(a-|\boldsymbol{r}'-\boldsymbol{R}_m|)\mathrm{d}\left(\boldsymbol{r}'-\boldsymbol{R}_m\right) \\
&\quad\approx \frac{\mathrm{i}}{4\pi a^2}\psi_\pm(\boldsymbol{R}_m) \\
&\qquad\times\int_0^a\left\{1+\mathrm{i}\frac{2}{\pi}\left(\ln r+\ln k+\gamma-\ln 2\right)\right\}2\pi r\,\mathrm{d}r \\
&\quad= -\frac{1}{4\pi}\left(2\ln\frac{ka}{2}+2\gamma-1-i\pi\right)\psi_\pm(\boldsymbol{R}_m). \qquad (9)
\end{aligned}$$

Therefore, when $\boldsymbol{r}$ is taken as $\boldsymbol{R}_m$ in equation (7), $G(\boldsymbol{R}_m,\boldsymbol{R}_m)$ is replaced by $-1/(4\pi)[2\ln(ka/2)+2\gamma-1-\mathrm{i}\pi]$.

Finally, the wavefunction $\psi_\pm(\boldsymbol{r})$ is expressed by

$$\begin{aligned}
\psi_\pm(\boldsymbol{r}) &= \oint\left[G(\boldsymbol{r},\boldsymbol{r}')\nabla'\psi_\pm(\boldsymbol{r}')-\psi_\pm(\boldsymbol{r}')\nabla'G(\boldsymbol{r},\boldsymbol{r}')\right]\cdot\boldsymbol{n}\,\mathrm{d}S' \\
&\quad+\sum_n\mathcal{G}(\boldsymbol{r},\boldsymbol{R}_n)\big(\mathcal{M}_\mp(\boldsymbol{R}_n)a^2\psi_\mp(\boldsymbol{R}_n) \\
&\quad\pm\mathcal{M}_z(\boldsymbol{R}_n)a^2\psi_\pm(\boldsymbol{R}_n)\big), \qquad (10)
\end{aligned}$$

where

$$\mathcal{G}(\boldsymbol{r},\boldsymbol{R}_n)\equiv\begin{cases}\dfrac{\mathrm{i}}{4}H_0^{(1)}\left(k|\boldsymbol{r}-\boldsymbol{R}_n|\right), & \boldsymbol{r}\neq\boldsymbol{R}_n\\ -\dfrac{1}{4\pi}\left(2\ln\dfrac{ka}{2}+2\gamma-1-\mathrm{i}\pi\right), & \boldsymbol{r}=\boldsymbol{R}_n.\end{cases} \qquad (11)$$

Thus, in order to involve the effect of the scatterers, we just sum up $\mathcal{G}(\boldsymbol{r},\boldsymbol{R}_n)(\mathcal{M}_\mp(\boldsymbol{R}_n)a^2\psi_\mp(\boldsymbol{R}_n)\pm\mathcal{M}_z(\boldsymbol{R}_n)a^2\psi_\pm(\boldsymbol{R}_n))$.

4. Rotation of magnetic moment

The 2D component of the magnetization at $\boldsymbol{R}_n$ can be expressed as

$$\mathcal{M}_\pm(\boldsymbol{R}_n)=\mathcal{M}_x(\boldsymbol{R}_n)\pm\mathrm{i}\mathcal{M}_y(\boldsymbol{R}_n)=\mathfrak{M}(\boldsymbol{R}_n)\exp(\pm\mathrm{i}\theta_{\boldsymbol{R}_n}). \qquad (12)$$

We consider the case that the 2D component of the magnetization rotates by the same angle δ within the x–y plane. Then, we have

$$\mathcal{M}'_\pm(\boldsymbol{R}_n)=\mathfrak{M}(\boldsymbol{R}_n)\mathrm{e}^{\pm\mathrm{i}(\theta_{R_n}+\delta)},$$

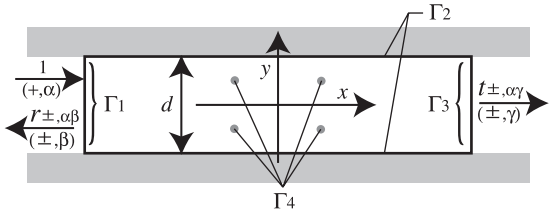

Figure 1. A model of a quantum wire with pointlike magnetic scatterers.

wherefore equation (10) can be rewritten as

$$\begin{aligned}
\psi_\pm(\boldsymbol{r}) &= \oint\left[G(\boldsymbol{r},\boldsymbol{r}')\nabla'\psi_\pm(\boldsymbol{r}')-\psi_\pm(\boldsymbol{r}')\nabla'G(\boldsymbol{r},\boldsymbol{r}')\right]\cdot\boldsymbol{n}\,\mathrm{d}S' \\
&\quad+\sum_n\mathcal{G}(\boldsymbol{r},\boldsymbol{R}_n)\big(\psi_\mp(\boldsymbol{R}_n)\mathfrak{M}(\boldsymbol{R}_n)\mathrm{e}^{\mp\mathrm{i}(\theta_{R_n}+\delta)} \\
&\quad\pm\psi_\pm(\boldsymbol{R}_n)\mathcal{M}_z(\boldsymbol{R}_n)\big) \\
\psi_\pm(\boldsymbol{r})\mathrm{e}^{\pm\mathrm{i}\frac{\delta}{2}} &= \oint\Big[G(\boldsymbol{r},\boldsymbol{r}')\nabla'\psi_\pm(\boldsymbol{r}')\mathrm{e}^{\pm\mathrm{i}\frac{\delta}{2}} \\
&\quad-\psi_\pm(\boldsymbol{r}')\mathrm{e}^{\pm\mathrm{i}\frac{\delta}{2}}\nabla'G(\boldsymbol{r},\boldsymbol{r}')\Big]\cdot\boldsymbol{n}\mathrm{d}S' \\
&\quad+\sum_n\mathcal{G}(\boldsymbol{r},\boldsymbol{R}_n)\Big(\psi_\mp(\boldsymbol{R}_n)\mathrm{e}^{\mp\mathrm{i}\frac{\delta}{2}}\mathfrak{M}(\boldsymbol{R}_n)\mathrm{e}^{\mp\mathrm{i}\theta_{R_n}} \\
&\quad\pm\psi_\pm(\boldsymbol{R}_n)\mathrm{e}^{\pm\mathrm{i}\frac{\delta}{2}}\mathcal{M}_z(\boldsymbol{R}_n)\Big) \qquad (13) \\
\tilde{\psi}_\pm(\boldsymbol{r}) &= \oint\left[G(\boldsymbol{r},\boldsymbol{r}')\nabla'\tilde{\psi}_\pm(\boldsymbol{r}')-\tilde{\psi}_\pm(\boldsymbol{r}')\nabla'G(\boldsymbol{r},\boldsymbol{r}')\right]\cdot\boldsymbol{n}\,\mathrm{d}S' \\
&\quad+\sum_n\mathcal{G}(\boldsymbol{r},\boldsymbol{R}_n)\Big(\tilde{\psi}_\mp(\boldsymbol{R}_n)\mathcal{M}_\mp(\boldsymbol{R}_n) \\
&\quad+\tilde{\psi}_\pm(\boldsymbol{R}_n)\mathcal{M}_z(\boldsymbol{R}_n)\Big),
\end{aligned}$$

where $\tilde{\psi}_\pm\equiv\psi_\pm\exp(\pm\mathrm{i}\delta/2)$ are defined. Thus, rotation of the whole magnetization never affects the quantum state.

In particular, supposing $M_z(\boldsymbol{R}_n)=0$ and the magnetization in the plane has turned in the same direction at every point, say $\theta_{\boldsymbol{R}_n}=\theta_c$, the integral equations depend only on the magnitude of magnetization $\mathfrak{M}(\boldsymbol{R}_n)$. It is easily confirmed by setting $\delta=-\theta_c$.

5. Application

Making use of equation (10), we can extend the BEM so as to deal with scattering problems by magnetic moments. Let us apply the extended BEM to a model of a quantum wire shown in figure 1. We assume that an electron wave of unit amplitude with up spin is incident from the left and the width of the quantum wire d is a length scale.

5.1. Numerical implementation

Supposing infinitely high potential outside the wire, the wavefunction vanishes on the wall, that is, the portion Γ_2. The

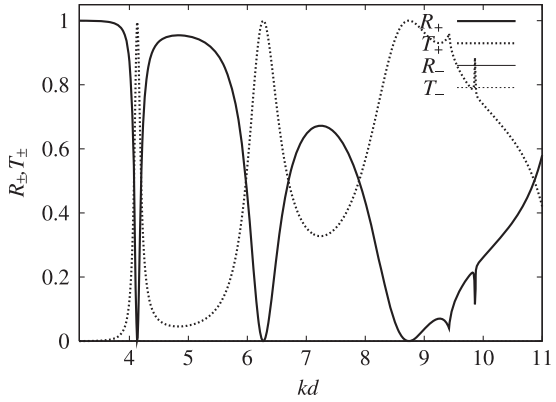

Figure 2. The reflection and transmission spectra of the quantum wire with four pointlike magnetic scatterers of $a = 0.05$, $\mathfrak{M}a^2 = 700$, $\mathcal{M}_z a^2 = 0$ and $\alpha = 1$.

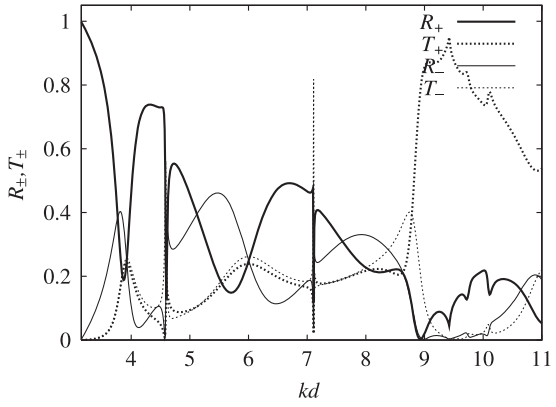

Figure 3. The reflection and transmission spectra of the quantum wire with four pointlike magnetic scatterers of $a = 0.05$, $\mathfrak{M}a^2 = 4$, $\mathcal{M}_z a^2 = 0$ and $\alpha = 1$.

wavefunctions on the portions Γ_1 and Γ_3 are expanded in terms of the eigenfunctions, respectively.

We can summarize the expression of the wavefunction on each portion as

$$\begin{aligned}
&\Gamma_1\colon \psi_\pm(\boldsymbol{r}) = \delta_{\pm,+}\sin\left(\frac{\alpha\pi}{d}\left(y+\frac{d}{2}\right)\right)\exp(\mathrm{i}k_\alpha x)\\
&\qquad + \sum_\beta r_{\pm,\alpha\beta}\sin\left(\frac{\beta\pi}{d}\left(y+\frac{d}{2}\right)\right)\exp(-\mathrm{i}k_\beta x)\\
&\Gamma_2\colon \psi_\pm(\boldsymbol{r}) = 0\\
&\Gamma_3\colon \psi_\pm(\boldsymbol{r}) = \sum_\gamma t_{\pm,\alpha\gamma}\sin\left(\frac{\gamma\pi}{d}\left(y+\frac{d}{2}\right)\right)\exp(\mathrm{i}k_\gamma x),
\end{aligned} \tag{14}$$

where $k_\alpha^2 = \sqrt{k^2 - (\alpha\pi/d)^2}$ and $\delta_{\pm,+}$ is the Kronecker delta symbol, being unity if $\delta_{+,+}$, otherwise zero. The quantities $t_{\pm,\alpha\gamma}$ and $r_{\pm,\alpha\beta}$ are the transmission and reflection coefficients of spin $\pm$, respectively.

On the portions Γ_1, Γ_2, Γ_3 and Γ_4, unknown variables are $r_{\pm,\alpha\beta}$, $\partial\psi_\pm/\partial n$, $t_{\pm,\alpha\gamma}$ and $\psi_\pm$, respectively. We solve simultaneous equations for these unknown variables. Then, we can calculate the wavefunction within a closed boundary by means of equation (10).

The reflection and transmission probability of up spin and down spin are defined by

$$R_\pm = \sum_\beta \frac{k_\beta}{k_\alpha}|r_{\pm,\alpha\beta}|^2, \qquad T_\pm = \sum_\gamma \frac{k_\gamma}{k_\alpha}|t_{\pm,\alpha\gamma}|^2. \tag{15}$$

5.2. Numerical results

As an example computation, a quantum wire with the same four magnetic scatterers is analyzed. We pay attention to the energy dependence of the transmission and reflection probabilities of each spin, that is transmission and reflection spectra. At first, we see the case of $a = 0.05$, $\mathfrak{M}a^2 = 700$, $\mathcal{M}_z a^2 = 0$ and incident mode $\alpha = 1$ as an example of a very large magnetization, shown in figure 2. The spectra of T_+ and R_+ in figure 2 have several peaks and dips. They are attributed to resonant tunneling phenomena. On the other hand,

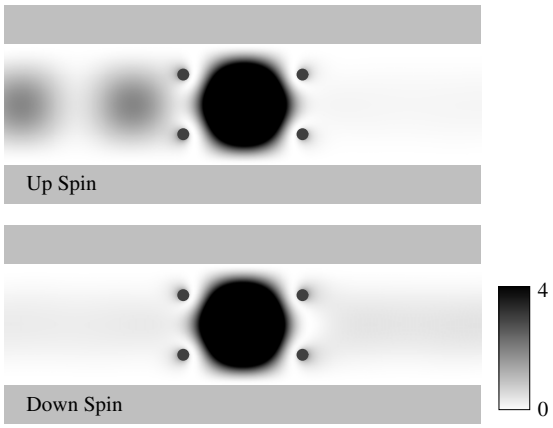

Figure 4. The density plots of the probability density of the up and down spin, $|\psi_\pm(\boldsymbol{r})|^2$ for $kd = 4.6$, where $R_+ \approx 0.12$, $T_+ \approx 0.15$, $R_- \approx 0.30$ and $T_- \approx 0.43$.

both R_- and T_- almost vanish. This fact means that the up spin and the down spin states are hardly coupled to each other. It is because, supposing the value of $\mathcal{M}_\mp(\boldsymbol{R}_n)$ is very large, the absolute values of $\psi_\mp$ near the point $\boldsymbol{R}_n$ should become small since they are determined consistently by equation (10). An electron cannot enter the domains of large magnetization. Therefore, it should be noted that a strong magnetic scatterer behaves just like a strong potential scatterer.

Now, we consider magnetization of smaller intensity. The reflection and transmission spectra for $a = 0.05$, $\mathfrak{M}a^2 = 4$ and $\mathcal{M}_z a^2 = 0$ are shown in figure 3. In this case, the spectra R_- and T_- take significant values and vary intricately, so that we see that the up and down spin states are coupled. The probability densities $|\psi_\pm|^2$ of up $(+)$ and down spin $(-)$ for $a = 0.05$, $\mathfrak{M}a^2 = 4$ and $\mathcal{M}_z a^2 = 0$ at peculiar points, that is, $kd = 4.6$, 7.11 and 9.42, are plotted in figures 4–6, respectively.

Figure 4 is for $kd = 4.6$ at which a very sharp dip appears in R_+. Here, we see a localized state trapped within the region surrounded four scatterers for each spin. The electron wave collides with the scatterers repeatedly, so that the transition in the opposite spin is enhanced. Furthermore, electrons of both

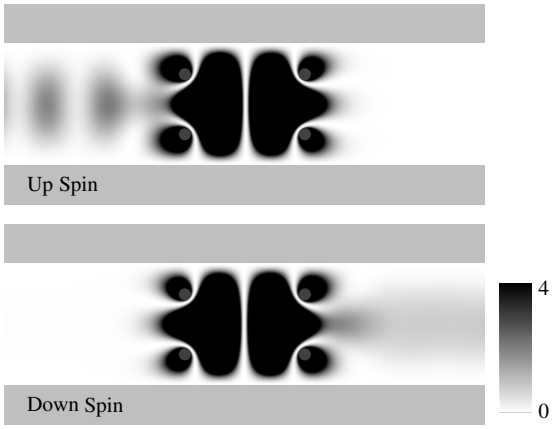

Figure 5. The density plots of the probability density of the up and down spin, $|\psi_{\pm}(\boldsymbol{r})|^2$ for $kd = 7.11$, where $R_+ \approx 0.14$, $T_+ \approx 0.01$, $R_- \approx 0.03$ and $T_- \approx 0.82$.

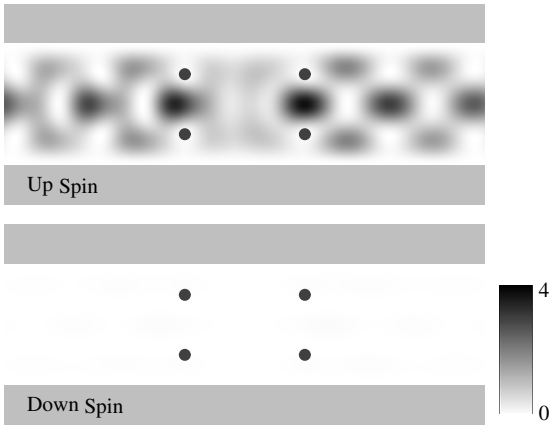

Figure 6. The density plots of the probability density of the up and down spin, $|\psi_{\pm}(\boldsymbol{r})|^2$ for $kd = 9.42$, where $R_+ \approx 0.05$, $T_+ \approx 0.95$, $R_- \approx 0.00$ and $T_- \approx 0.00$.

spins are localized on the sites of the scatterers. This is the evidence that spin flip-flop of electrons occurs resonantly.

The probability densities for $kd = 7.11$, where a very sharp peak is seen in T_-, is presented in figure 5. In this case, more than 80% of the incident wave transmits to the right by the down spin. It should be noted that the probability densities take remarkably large values around each scatterer. The electron wave is localized within the surrounded region for each spin as well as in figure 4, whereas we see a nodal line. This fact makes us confirm that major peaks at both $kd = 4.6$ and $kd = 7.11$ are attributed to the interference in the longitudinal direction.

Now, we turn to discuss the cause of the slightly broader minor peak at $kd = 9.42$. At the peak, the transmission probability of up spin reaches 95%. In figure 6, the probability densities for $kd = 9.42$ are shown. Here, we see that the probability density of the up spin takes very small values around the scatterers and has large values between the scatterers even in the transverse direction. This means that the electron wave merely feels the scatterers, so that it propagates almost freely. Therefore, the wavenumber $kd = 9.42$ is

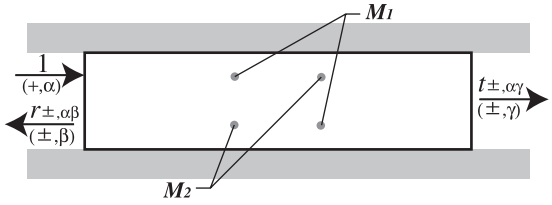

Figure 7. Asymmetric configuration of magnetic scatterers with $M_1 = (0, m, 0)$ and $M_2 = (m, 0, 0)$.

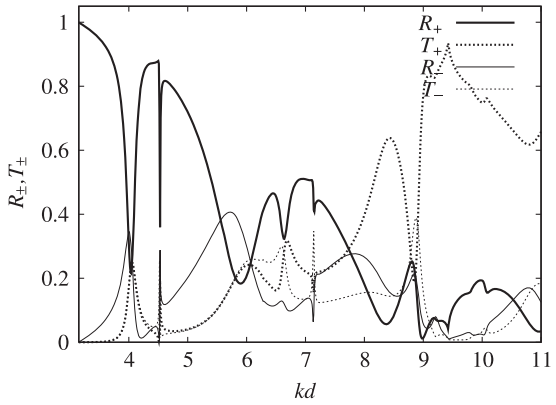

Figure 8. The reflection and transmission spectra of the asymmetric configuration for $a = 0.05$ and $ma^2 = 4$.

attributed just to that of the fundamental stationary mode between the scatterers located in a line with the transverse direction.

It is considered that the existence of these localized states evidently originates in the symmetry among scatterers. In order to confirm that, we consider an asymmetric configuration of magnetic scatterers as shown in figure 7. Namely, the direction of two of the magnetic moments is changed. Figure 8 shows the reflection and transmission spectra for $a = 0.05$, $ma^2 = 4$ and $\alpha = 1$. The major property is similar to that of figure 3. However, the peaks and dips which are considered to correspond to those in figure 3 shift to the lower side and become shallow. Several new peaks and dips appear, which cannot be seen in figure 3. For example, at $kd = 8.37$, a new valley in T_+ appears. The density plots of $|\psi_{\pm}|^2$ for $kd = 8.37$ are shown in figure 9. The probability density of the down spin shows that the state is localized within the domain surrounded by the four scatterers and has a nodal line in the longitudinal direction and the transverse direction, respectively.

5.3. Calculation accuracy and calculation cost

In finishing this section, calculation accuracy and calculation cost should be mentioned.

Conservation of probability is employed in order to evaluate the accuracy of the numerical calculation. We have already performed calculations in many cases including ones of complicated boundary shapes by means of this method. Surprisingly, an error of the order of 0.1% in conservation of probability is realized for all of them in spite of the approximation.

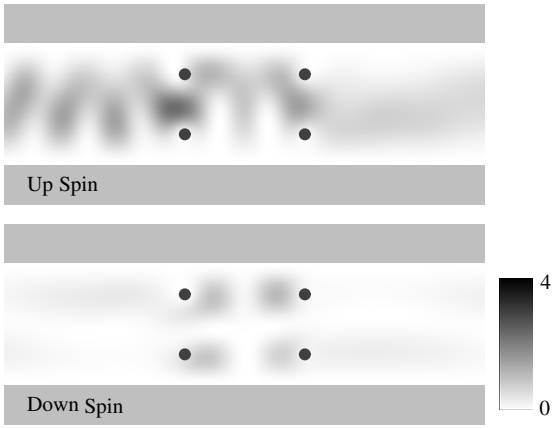

Figure 9. The density plot of $|\psi_{\pm}(r)|^2$ for $kd = 8.37$, where $R_+ \approx 0.05$, $T_+ \approx 0.63$, $R_- \approx 0.17$ and $T_- \approx 0.15$.

The boundary is discretized into segments of 500 in typical calculations shown in the present paper, where the length of a segment is smaller than 1/8 of the wavelength. Then, the CPU time needed to solve simultaneous equations about the unknown variables on the boundary for a certain value of kd is 15 min using a PC driven by a 3 GHz Pentium 4 processor with a Intel FORTRAN compiler under Linux. Values of a wavefunction within the boundary on a grid of 250×1000 are calculable in 1.5 h.

These facts encourage us to apply this method to more practical problems.

6. Conclusions and discussions

In the present paper, the boundary element method has been extended in order to treat 2D ballistic electron systems including a lot of pointlike magnetic scatterers. By modeling the shape of a magnetic scatterer by a cylinder of very small radius, we have performed the (2D) volume integral including a wavefunction, Green function and magnetization, so that we have derived the simultaneous integral equations in which the up and down spin are coupled. In numerical implementations, the equations have been discretized in terms of the boundary element method.

The extended method has been applied to the concrete problem, and it has been confirmed that the method realizes very high calculation accuracy in spite of the approximation. Thus, the method proposed here is powerful, convenient and accurate to analyze the transport property of an electron system with a number of small magnetic obstacles. Moreover, the method is easily extended to a case in the presence of a uniform magnetic field by combining with the method reported in [16]. The examples of applications are just a demonstration of the method developed here, whereas the physically interesting phenomena have also been discussed. Namely, it has been shown that too strong a magnetization never makes the up and the down spin states couple and that several weak pointlike magnetic moments are enough to flip the spin state of a propagating electron wave. Further physical analyses and applications are now in progress. The results will be reported elsewhere in the very near future.

Acknowledgments

This work was partly supported by the 21st century COE program 'Frontiers of Super-Functionality Organic Devices' from the Japanese Ministry of Education, Culture, Sports, Science and Technology.

References

[1] Imamura H, Kobayashi N, Takahashi S and Maekawa S 2000 *Phys. Rev. Lett.* **84** 1003
[2] Maekawa S and Shinjo T 2002 *Spin Dependent Transport in Magnetic Nanostructures* (London: Taylor and Francis)
[3] Wolf S A, Awschalom D D, Daughton R A, von Molnar S, Roukes M L, Chtchelkanova A Y and Treger D M 2001 *Science* **294** 1488
[4] Folk J A, Potok R M, Marcus C M and Umansky V 2003 *Science* **299** 679
[5] Elzerman J M, Hanson R, Willems van Beveren L H, Witkamp B, Vandersypen L M K and Kouwenhoven L P 2004 *Nature* **430** 431
[6] Slonczewski J C 1989 *Phys. Rev.* B **39** 6995
[7] Song J F, Ochiai Y and Bird J P 2003 *Appl. Phys. Lett.* **82** 4561
[8] Weiss D, Roukes M L, Menschig A, Grambow P, von Klitzing K and Weimann G 1991 *Phys. Rev. Lett.* **66** 2790
[9] Nihey F, Hwang S W and Nakamura K 1995 *Phys. Rev.* B **51** 4649
[10] Schuster R, Ensslin K, Kotthaus J P, Böhm G and Klein W 1997 *Phys. Rev.* B **55** 2237
[11] Xue D P and Xiao G 1992 *Phys. Rev.* B **45** 5986
[12] Yagi R and Iye Y 1993 *J. Phys. Soc. Japan* **62** 1279
[13] Peeters F M and Vasilopoulos P 1993 *Phys. Rev.* B **47** 1466
[14] Kato M, Endo A, Katsumoto S and Iye Y 1998 *Phys. Rev.* B **58** 4876
[15] Ueta T 2002 *Electron. Commun. Japan* II **85** 1
[16] Ueta T 1999 *Phys. Rev.* B **60** 8213
[17] Abramowitz M and Stegun I A (ed) 1972 *Handbook of Mathematical Functions* (New York: Dover) pp 358–60